Chemical and Electrical Passivation of Single-Crystal Silicon(100) Surfaces through a Two-Step Chlorination/Alkylation Process

E. Joseph Nemanick, Patrick T. Hurley, Lauren J. Webb, David W. Knapp, David J. Michalak, Bruce S. Brunschwig, and Nathan S. Lewis*

210 Noyes Laboratory, 127-72, Division of Chemistry and Chemical Engineering, Kavli Nanoscience Institute, California Institute of Technology, Pasadena, California 91125

Single-crystal Si(100) surfaces have been functionalized by using a two-step radical chlorination–Grignard (R= MgCl, R = CH$_3$, C$_2$H$_5$, C$_4$H$_9$, C$_6$H$_5$, or CH$_2$C$_6$H$_5$) alkylation method. After alkylation, no chlorine was detectable on the surface by X-ray photoelectron spectroscopy (XPS), and the C 1s region showed a silicon-induced peak shift indicative of a Si–C bond. The relative intensity of this peak decreased, as expected, as the steric bulk of the alkyl increased. Despite the lack of full alkyl termination of the atop sites of the Si(100) surface, functionalization significantly reduced the rate of surface oxidation in air compared to that of the H-terminated Si(100) surface, with alkylated surfaces forming less than half a monolayer of oxide after over one month of exposure to air. Studies of the charge-carrier lifetime with rf photoconductivity decay methods indicated a surface recombination velocity of <30 cm s^{-1} for methylated surfaces, and <60 cm s^{-1} for Si surfaces functionalized with the other alkyl groups evaluated. Soft X-ray photoelectron spectroscopic data indicated that the H–Si(100) surfaces were terminated by SiH, SiH$_2$, and SiH$_3$ species, whereas Cl–Si(100) surfaces were predominantly terminated by monochloro (SiCl and SiHCl) and dichloro (SiCl$_2$ and SiHCl$_2$) Si species. Methylation produced signals consistent with termination by Si–alkyl bonding arising from SiH(CH$_3$)-, SiH$_2$(CH$_3$)-, and Si(CH$_3$)$_2$-type species.

I. Introduction

Interest in silicon functionalization emanates from a desire to passivate the Si surface to protect against oxidation by air and/or water and to prevent charge-carrier recombination. Silicon–carbon covalent bonds are a potentially attractive passivation layer. The silicon–carbon bond is kinetically stable, which reduces the reactivity of the alkylated surface toward oxygen, thus preventing the formation of oxide and retarding the formation of charge-carrier recombination sites at the bulk silicon–surface interface. Many methods have emerged for functionalization of Si through the use of covalently attached organic groups.[1–4] Functionalization with Si–C bonds has attracted much attention due to the kinetic stability of the Si–C bond as well as the versatility of introduction of organic functionality using straightforward extensions of organosilane chemistry. An early functionalization technique for the formation of Si–C bonds used the H-terminated Si(111) surface to react with unsaturated alkenes, through a radical process catalyzed by a diacyl peroxide initiator.[5,6] This reaction yielded both Si–C bonds and surface oxidation, suggested to be in the form of Si–OH bonds. The reaction was further refined by use of ultraviolet (UV)[7–9] or white[10] light, thermal energy,[11,12] transition metal complexes,[13] and Lewis acids[14–16] to catalyze the reaction, and was expanded to encompass the Si(100)[11,12] surface as well as porous silicon.[10] Functionalization of silicon surfaces has subsequently expanded to encompass electrochemical functionalization,[17,18] radical halogenation,[19] and transmetalation with alkyl Grignard and lithium reagents.[19–21]

The H-terminated Si(111) surface prepared by etching Si in NH$_4$F(aq) has well-ordered terraces of silicon atoms that span hundreds of nanometers, with only a single Si–H bond per Si atop (or surface) site.[22,23] Modification of such H-terminated Si(111) surfaces by using a two-step chlorination–alkylation process has been shown to produce electrically and chemically stable surfaces.[21,24,25] Chemically etched Si(100) surfaces, however, cannot be prepared as cleanly as the H–Si(111) surface. Fluoride etches of the Si(100) surface produce several surface Si hydride species including SiH, SiH$_2$, and SiH$_3$, and leave the surface rough on an atomic scale.[22,23,26] Passivation of this chemically diverse surface presents a significant challenge. On the Si(111) surface, each silicon atop atom has only one Si–H bond, which is normal to the surface. Thus in principle alkylation with small groups such as methyl can yield one alkyl group per Si surface atom. However, when larger alkyl groups are used, steric crowding will limit the number of surface atoms that can be modified.[27] For the Si(100) surface, a single surface silicon atom can have multiple Si–H bonds, and not all the bonds are normal to the surface. Thus it will not be possible to alkylate all Si–H sites even with small alkyl groups.

In this study, single-crystal (100)-oriented Si surfaces were first chlorinated by using PCl$_5$ in a radical reaction followed by reaction with alkyl Grignard reagents at temperatures above the boiling point of the Grignard solvent. Short-chain alkyl groups (–CH$_3$, –C$_2$H$_5$, and –C$_4$H$_9$), as well as the bulkier group phenyl (–C$_6$H$_5$), were used. Surface recombination velocities (*S*) for photogenerated charge carriers were measured through rf conductivity decay methods. X-ray photoelectron spectroscopy (XPS) of the samples with both "soft" (140 eV) and "hard" (1486.6 eV) X-rays was employed to characterize the surface after functionalization, as well as to measure the oxidation of the surfaces after exposure to an air ambient.

Single-Crystal Silicon(100) Surfaces

J. Phys. Chem. B, Vol. 110, No. 30, 2006 **14771**

II. Experimental Section

A. Silicon Alkylation. Silicon wafers were (100)-oriented, 270 ± 25 μm thick, n-type, phosphorus-doped samples, with a resistivity of $1-6$ kΩ cm (Virginia Semiconductor Inc.). The samples for oxidation studies as well as electrical passivation measurements were obtained from high-purity, float-zone-grown, double-side polished, Si(100) wafers. Except as noted, all reagents used were ACS reagent grade, were stored in a N_2-(g)-purged glovebox, and were used as received. Water rinses used 18 MΩ cm resistivity water obtained from a Barnsted Nanopure system.

Silicon samples were scribed into squares averaging 0.7 cm on a side and were handled by the edges with Teflon tweezers. Samples covered with native oxide were first cleaned by sequential sonication in methanol, acetone, dichloromethane, 1,1,1-trichloroethane, dichloromethane, acetone, and methanol (VWR Scientific Products, West Chester, PA) for 3 s each. Samples were then rinsed in H_2O and etched in buffered HF (pH 5, Transene Corp., Danvers, MA) for 30 s. Samples were then removed and rinsed in water for <2 s per side to limit oxidation, and dried in flowing N_2(g) for 10 s. The samples were then passed into a N_2(g)-atmosphere glovebox for functionalization.

To chlorinate the surfaces, the H-terminated Si(100) samples were placed into septum-capped test tubes and exposed for 1 h at 95 °C to chlorobenzene saturated with PCl_5 (99.998% Strem, Newburyport, MA). A small amount (<1 mg) of benzoyl peroxide (97%, Aldrich Chemical Corp.) was added to initiate chlorination of the surface. For XPS measurements of the chlorinated surface, samples were rinsed in tetrahydrofuran (THF) and dried under flowing N_2(g). Samples for 1.5 keV XPS analysis were then passed without exposure to air through a load lock directly into an ultrahigh-vacuum (UHV) XPS chamber. After chlorination, the samples were washed in anhydrous THF (99.8%, inhibitor free, Aldrich) and were placed in Teflon glass reaction flasks that were sealed with screw caps. The flasks contained 10 mL of anhydrous THF and 10 mL of a 1 M Grignard reagent in THF. The Grignard reagents were either CH_3MgCl, CH_3CH_2MgCl, $CH_3(CH_2)_3MgCl$, C_6H_5MgCl, or $C_6H_5CH_2MgCl$. The reaction solution was heated to $110-120$ °C for 21 h in a sealed reaction vessel. After reaction, samples were rinsed in THF followed by anhydrous methanol (99.8% Aldrich), removed from the glovebox, and sonicated in a 5 mL solution of methanol and glacial acetic acid (10:1) (Aldrich) for 5 min to remove any adsorbed magnesium salts. Samples were then rinsed with 18 MΩ cm resistivity H_2O and either passed directly into the UHV load lock for XPS analysis (1.5 keV) or placed in scintillation vials for surface recombination velocity measurements.

B. X-ray Photoelectron Spectroscopy Measurements. XPS data were collected on a UHV system that has been described previously[28] with 1486 eV X-rays from an Al Kα source. The spectrometer resolution was ~0.5 eV for the high-resolution scans and ~ 1.0 eV for the survey scans. All energies are reported as binding energies in eV, with data analysis as described previously.[24,27] The XPS system was periodically calibrated by using the 4f peaks at 83 and 87 binding eV, respectively, of a Au standard.

Samples were first scanned from 0 to 1000 eV binding energy to monitor signals for Cl, C, and O. The Si 2p, Cl 2p, and C 1s regions of $98-105$, $198-204$, and $282-287$ eV binding energy, respectively, were investigated in detail. Scan times of up to 4 h were employed for data collection.

The fractional monolayer coverage of oxide species on the surface was determined by using the substrate-overlayer model.[29] Data from the carbon 1s emission region were fitted to Voigt functions having 70% Gaussian and 30% Lorentzian character. Three functions were used, representing silicon-bonded carbon at 283.9 eV, carbon-bonded carbon at 285.0 eV, and oxygen-bonded carbon at 286.8 eV.[27,30,31] The peak centers were allowed to float, though the center-to-center distances were fixed at 1.1 eV between the silicon-bonded carbon and the carbon-bonded carbon emissions, and at 1.8 eV between the oxygen-bonded carbon and the carbon-bonded carbon emissions. The integrated area under each carbon peak was ratioed to the integrated area under the silicon 2p peaks for that sample and normalized for scan time. The ratio of the silicon-bonded carbon to the normalized area for the Si 2p peak, C_{Si}/Si, was then compared between alkylated surfaces. Surface coverages for each alkyl group are reported relative to the value of C_{Si}/Si observed for CH_3-terminated Si(100) surfaces. Error estimates for the measurements were taken from previous studies.[27]

C. Infrared Spectroscopy. For IR spectroscopy, n-type, phosphorus-doped, float-zone, single-crystal, 505 ± 25 μm thick Si(100) wafers (Silicon Valley Microelectronics Inc., Santa Clara, CA) with a resistivity of >30 Ω cm were cut into 2.1 cm × 3 cm segments. Samples were cleaned with an RCA etch, before a final etch in degassed buffered HF (pH 5) for 30 s. Surfaces were chlorinated and alkylated as described above, with samples sealed under N_2(g) for transport to the Fourier Transform (FT)-IR spectrometer. Samples were unsealed and placed in a grazing angle (65°) attenuated total reflectance (GATR) mount (Harrick Scientific Products Inc., Pleasantville, NY). The GATR mount was placed in a Vertex 70 FT-IR spectrometer (Bruker Optics Inc., Billerica, MA) for measurements. A total of 512 scans for each sample were taken in air, with background scans of air subtracted from the spectra.

D. Soft X-ray Photoelectron Spectroscopy. Soft X-ray experiments were performed at Brookhaven National Laboratory on the U4A beamline at the National Synchrotron Light Source. Samples were prepared and data were collected as described previously.[32] Samples were prepared in an inert atmosphere box but had to be exposed to air for <5 min for transfer into the spectrometer. Samples were sufficiently conductive that no charging-induced peak shifts were observed.

For data analysis, a Shirley background was subtracted from the spectra to allow for peak fitting. The Si $2p_{1/2}$ component peaks were then removed from the spectra by subtraction of a peak 0.6 eV higher in energy and 0.51 the size of each Si $2p_{3/2}$ peak.[32] Residual spectra were fitted to modified Voigt functions with peak shapes that were 95% Gaussian and 5% Lorentzian. All peak positions are given relative to the bulk Si 2p emission.

By using a simplified substrate-overlayer model, the sum of all surface species present was assigned to one monolayer as a tool for distinguishing between equivalent local minima on the peak fitting surface. This model gives the surface density of an individual species, $\Gamma_{Si,surf}$, as derived from the ratio of the surface Si 2p signal for that species relative to the area of the bulk Si 2p signal. The peak area ratio for the surface and bulk species ($I_{Si,surf}/I_{Si,bulk}$) is equal to

$$\frac{I_{Si,surf}}{I_{Si,bulk}} = \frac{\Gamma_{Si,surf}}{n_{Si,bulk}l_{Si} - \Gamma_{Si,surf}} \tag{1}$$

In this expression, $n_{Si,bulk}$ is the number density of bulk crystalline Si atoms (5.0×10^{22} cm^{-3})[33] and l_{Si} is 3.5 Å.
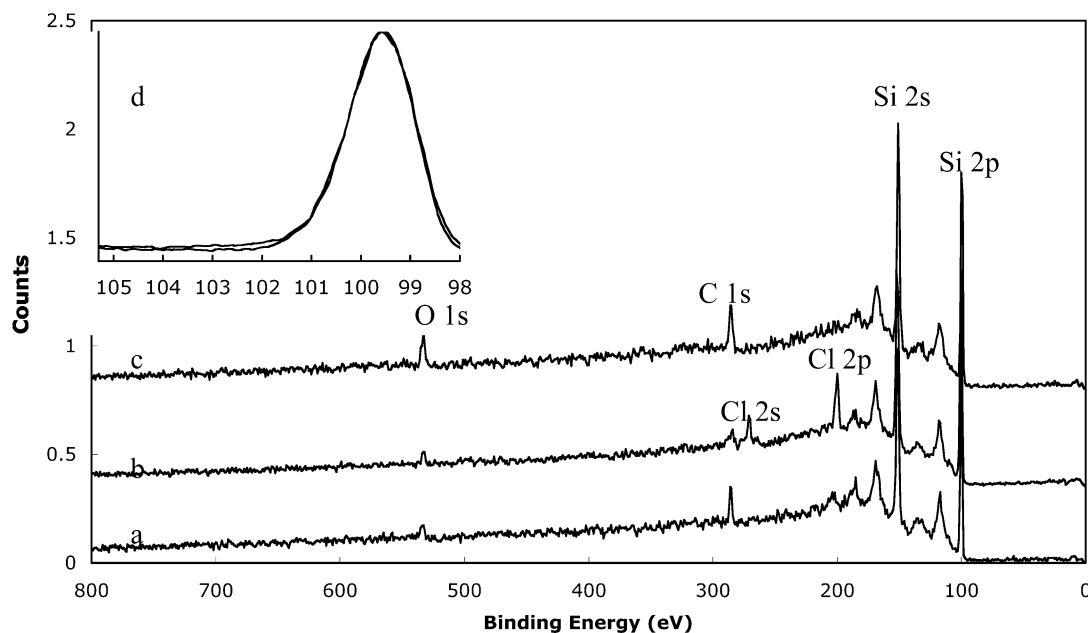
Figure 1. XPS survey spectra (1.5 keV) for Si(100) surfaces: (a) freshly etched H-terminated silicon surface, (b) chlorinated Si surface, and (c) methylated Si surfaces. (d) High-resolution scan of the Si 2p region of a CH$_3$-terminated surface (lower line), and the Si 2p region of a surface with 0.2 monolayer of oxide (upper line) as determined from the area of the oxidized Si 2p signal relative to the bulk Si 2p signal.

Substituting $I = I_{Si,surf}/I_{Si,bulk}$ and $\Gamma_{Si,bulk} = n_{Si,bulk}l_{Si}$ into eq 1 and rearranging yields

$$\Gamma_{Si,surf} = \frac{I}{1 + I}\Gamma_{Si,bulk} \qquad (2)$$

Dividing the calculated value of $\Gamma_{Si,surf}$ by the number density of atop sites on the Si(100) surface, 6.9×10^{14} cm^{-2},[34] gives the monolayer coverage of modified Si atoms. The distance between Si layers along a vector perpendicular to the Si(100) crystal face is 1.36 Å,[35] implying that an electron escape depth of 3.5 Å will sample $\approx$ 2.6 monolayers of the Si crystal.

E. Surface Recombination Velocity Measurements. Surface recombination velocity measurements were collected as described previously, using a contactless rf conductivity apparatus.[21] The absorbed rf signal was recorded by averaging 128 traces. Data were fitted to a single-exponential decay:

$$A = y_o + ae^{-t/\tau} \qquad (3)$$

where τ is the observed charge-carrier lifetime. The surface recombination velocity, S, was obtained from τ through

$$\frac{1}{\tau} = \frac{1}{\tau_b} + \frac{2S}{d} \qquad (4)$$

where τ_b is the bulk lifetime, and d is the sample thickness. For all measurements, $\tau_b \gg \tau$, so $S \approx d/2\tau$.

All τ values are reported after the first 24 h following alkylation. Measurements of τ for an individual sample showed an increase in charge-carrier lifetime over the first day, but stabilized thereafter. To monitor the stability of the alkylated surface toward oxidation, samples were stored in scintillation vials under laboratory air and normal laboratory illumination conditions for up to 11 months, and τ values were monitored periodically during this time interval.

III. Results

A. X-ray Photoelectron Spectroscopy. Figure 1 shows representative survey-scan XPS data for the two-step chlorina-

tion/alkylation of Si(100) surfaces. Freshly etched H-terminated surfaces, spectrum a, exhibited peaks for elemental Si 2s at 150 eV and Si 2p at 100 eV as well as the Si phonon absorption bands at 17 and 36 eV above the Si 2s and Si 2p peaks, respectively. Trace amounts of C and O were observed at 284 and 532 eV. Cl 2p and 2s peaks, at 201 and 271 eV, respectively, appeared only after the chlorination reaction, spectrum b. After alkylation with CH$_3$MgCl, spectrum c, the Cl 2s and 2p peaks disappeared from the spectrum, as has been observed previously for Si(111) surfaces,[19,28] and the C 1s and O 1s peaks increased in amplitude.

An upper limit on the coverage of SiO$_2$ can be estimated from the intensity of the O 1s peak relative to the intensity of the Si 2p signal. Use of the substrate-overlayer method,[29] in which the area under the O 1s peak, $I_{O\,1s}$, relative to the area of the Si 2p peak, $I_{Si\,2p}$, is multiplied by the ratio of the sensitivity factors of silicon (SF$_{Si\,2p}$ = 0.817) and oxygen (SF$_{O\,1s}$ = 2.93) and by the number density of a monolayer of Si atoms on the (100) surface, Γ_{Si}, and correcting for the escape depth of Si 2p photoelectrons in Si, λ_{Si}, as well as the stoichiometry factor for SiO$_2$ (0.5):

$$\Gamma_{SiO_2} = 0.5\left(\frac{I_{O\,1s}}{\lambda_{Si}I_{Si\,2p}}\right)\left(\frac{SF_{Si\,2p}}{SF_{O\,1s}}\right)\Gamma_{Si} \qquad (5)$$

yields an upper limit of 0.2 monolayer (ML) of SiO$_2$ for the CH$_3$-terminated surface in Figure 1c, assuming that all of the oxygen 1s signal arises from SiO$_2$.

Figure 2 shows a high-resolution XPS scan of the C 1s region of a C$_2$H$_5$-functionalized Si(100) surface. Two main emissions, at 284.1 and 285.3 eV, were observed, with a third, small signal at 286.9 eV. The emissions located at 285.3 and 286.9 eV were also observed on H-terminated Si(100) surfaces, whereas the low binding energy emission at 284.1 eV was unique to alkylated Si surfaces. The 284.1 eV peak can thus be assigned to emission of core level electrons of C atoms covalently bonded to the relatively electropositive Si.[7,31,36] The higher energy emission at 285.3 eV can be ascribed to carbon bonded to either hydrogen or another carbon atom. This carbon peak was the

Single-Crystal Silicon(100) Surfaces

J. Phys. Chem. B, Vol. 110, No. 30, 2006 **14773**
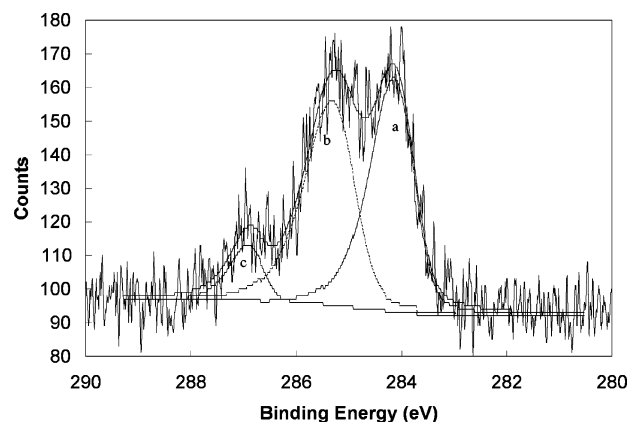
Figure 2. XPS spectrum (1.5 keV) for the C 1s region for a CH₃-terminated Si(100) surface. The data have been fitted with Voigt functions. The fitted peaks are assigned to (a) carbon atoms bonded to silicon (C_{Si}) (dashed line), (b) carbon atoms bonded to carbon and hydrogen (dotted line), and (c) carbon atoms bonded to oxygen (from adventitious sources) (solid line).
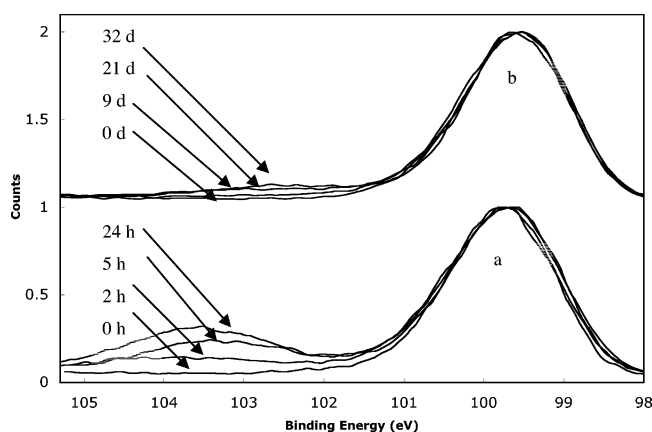

Figure 3. XPS spectra (1.5 keV) for the Si 2p region showing the relative oxidation of the surface for (a) H-terminated Si (100) after 0, 2, 5, and 24 h and (b) CH₃-terminated Si (100) after 0, 9, 21, and 32 days.

sum of C 1s electrons from adventitious carbon sources as well as alkylated carbons that do not participate in the Si−C bond. The third C 1s peak, at higher binding energy 286.9 eV, is ascribed to adventitious carbon bonded to oxygen from the THF solvent used in functionalization, or from carbonaceous materials present in the laboratory environment. The two peaks at higher energy may also contain contributions from vibrational excitations associated with the lower energy peaks.[36]

The C 1s peak at 284.1 eV (C_{Si}) provides semiquantitative information on the relative coverage of surficial Si−C bonds for the various alkylated surfaces. This peak is useful for providing an estimate of the alkyl coverage because, unlike the infrared spectra in the C−H stretching region, interpretation of the intensity of this low-energy C 1s peak is not confounded by the presence of adventitious hydrocarbons on the Si surface. The peak area ratio of the C_{Si} peak to the Si 2p signal (C_{Si}/Si) was measured relative to the C_{Si}/Si peak area ratio for the CH₃-terminated Si(100) surface. Ethylated Si(100) surfaces showed a C_{Si}/Si peak ratio of 60% relative to CH₃-terminated Si(100) surfaces, whereas the larger alkyl groups, phenyl and octyl, exhibited lower Si−C coverage, and the still bulkier isopropyl and *tert*-butyl groups produced signals that were only 30% of the C_{Si}/Si peak ratio of CH₃-terminated Si(100) (Table 1).

Figure 3a presents the oxidation of cleaned and etched Si-(100) surfaces exposed to laboratory air and illumination for
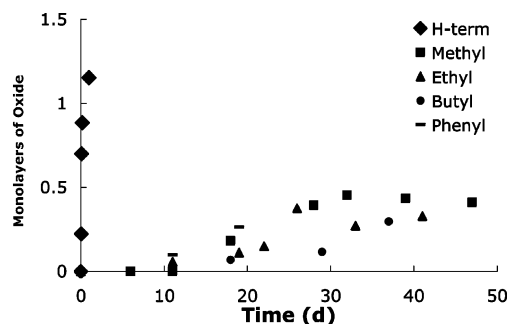
Figure 4. Plot of surface oxide growth for H-terminated and alkylated Si(100) surfaces vs time in air as measured by XPS.

TABLE 1: C_{Si}/Si XPS Integrated Area Ratios for Alkylated Si(100) Surfaces Showing the Relative Amount of Carbon Bonded to Silicon for Each Alkylated Surface

	ratio C_{Si}/Si	fraction of −CH₃ coverage
methyl	0.14 ± 0.02	
ethyl	0.09 ± 0.02	0.6 ± 0.2
phenyl	0.06 ± 0.02	0.4 ± 0.2
octyl	0.07 ± 0.02	0.5 ± 0.2
isopropyl	0.04 ± 0.02	0.3 ± 0.2
tert-butyl	0.04 ± 0.02	0.3 ± 0.2

24 h, showing the progressive oxidation of the surface. Neither the H-terminated nor CH₃-terminated Si(100) surfaces initially had measurable oxidized Si, with less than 0.1 ML of SiO₂, based on the readily detectable area of a peak in the high binding energy portion of the Si 2p region (Figure 1d).

The H-terminated Si(100) surface oxidized rapidly over the course of 24 h, yielding an integrated peak area equivalent to 1.1 monolayers of Si oxide. The broad, oxygen-shifted, Si 2p peak at ∼103.5 eV was assigned to a combination of Si^{4+} and Si^{3+} from SiO_x on the surface. The region from 101 to 102 eV showed small signals, indicating a paucity of lesser oxides such as Si^{1+} or Si^{2+}. In contrast, Figure 3b presents the oxidation of a CH₃-terminated Si(100) surface, showing surface oxidation at a greatly reduced rate, reaching only 0.44 monolayer of oxide after over 32 days. A comparison of the oxides shows that the oxide peak for the oxidized CH₃-terminated Si(100) surface occurred at a lower binding energy than that for the oxidized H-terminated Si(100) surface, implying the formation of a relatively higher fraction of lower order oxides, such as Si^{1+} and Si^{2+}, on oxidized CH₃−Si(100) surfaces.

Si(100) surfaces functionalized with larger alkyl groups showed the same reduction in oxidation rate relative to the H-terminated Si(100) surface. Figure 4 depicts the monolayer equivalents of SiO₂ that formed on alkylated and H-terminated surfaces during >45 days of exposure to laboratory air and illumination. All functionalized surfaces exhibited <0.5 monolayer of SiO₂ after one month. No discernible trend was observed in surface oxidation as a function of the identity of the alkylating group.

B. Infrared Absorbance Spectroscopy. Figure 5 shows ATR infrared absorbance spectra of the (100)-oriented Si surfaces alkylated with −CH₃ and −C₂H₅ groups, as well as spectra of the etched, H-terminated Si(100) surface. The H-terminated surface showed a multipart peak, corresponding[22,23] to the Si−H stretches for Si−H groups at ∼2080 cm⁻¹, HSi−H groups at 2120 cm⁻¹, and H₂Si−H groups at 2140 cm⁻¹. After chlorination and alkylation, broad peaks associated with Si−Hₓ stretches were observed for surfaces alkylated with methyl and ethyl groups, indicating that at least some of the chlorinated surface sites were terminated with H atoms. The broadening of these
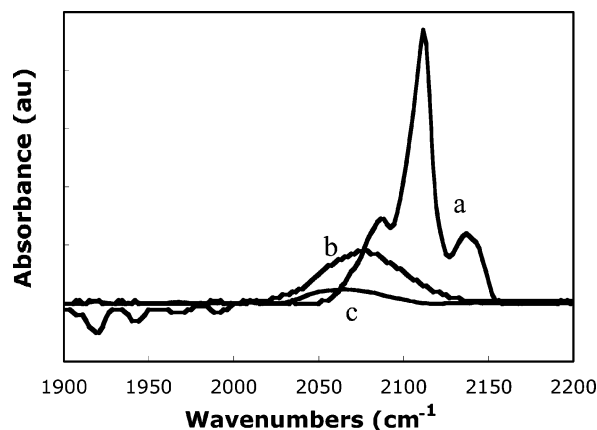
Figure 5. Infrared absorbance spectra for (a) H-terminated Si(100) surface, (b) C_2H_5-terminated Si(100) surface, and (c) CH_3-terminated Si(100) surface.

TABLE 2: Charge Carrier Lifetimes and Surface Recombination Velocities As Measured by Radio Frequency Photoconductivity Decay

|	τ (μs)	S (cm s^{-1})
methyl	$(5 \pm 2) \times 10^2$	$(3 \pm 1) \times 10^1$
ethyl	$(2 \pm 1) \times 10^2$	$(6 \pm 2) \times 10^1$
butyl	$(2 \pm 1) \times 10^2$	$(6 \pm 2) \times 10^1$
phenyl	$(3 \pm 1) \times 10^2$	$(5 \pm 3) \times 10^1$
H-terminated	<10	>10^3

peaks is likely due to the heterogeneous steric envrionments around the Si−H sites. The existence of both edge and surface sites and both Si−H and Si−R terminating bonds allows for the formation of many different R_aSiH_b species, where $a, b =$ 0, 1, and 2. Further interaction between different neighbors will result in small shifts and a broadening of the observed spectra in the IR absorbance.

C. Surface Recombination Velocity Measurements. Photogenerated charge-carrier lifetimes, τ, as measured by rf conductivity decay, for air-exposed H-terminated Si(100) surfaces were extremely low, $\tau < 10$ μs. Assuming negligible recombination in the bulk, the charge-carrier lifetimes were dominated by diffusion of photogenerated charge carriers to the sample surface, indicating a surface recombination velocity, S, of >1000 cm s^{-1}. These samples showed no measurable change in charge-carrier lifetime after prolonged exposure to atmosphere.

Alkyl-functionalized Si(100) surfaces showed substantial improvements in charge-carrier lifetime relative to the H-terminated surface, indicating a large reduction of surface recombination. Table 2 shows the τ and S values measured for the various alkylated samples after 4 days in air. In all cases the alkylated samples had significantly smaller values of S than the air-exposed H-terminated Si(100) surfaces, with the CH_3-terminated surfaces having the smallest S values.

The charge-carrier lifetimes of all samples, after an initial increase in the first 4 days, remained stable over extended periods of time. This increase in the lifetimes for the alkylated samples was reproducible over a range of sample preparations and conditions. After 11 months in capped, air-filled vials located on a laboratory benchtop, CH_3-terminated samples displayed $\tau = (4 \pm 1) \times 10^2$ μs, H_5C_2-terminated samples showed $\tau = (2 \pm 1) \times 10^2$ μs, and H_9C_4-terminated samples showed $\tau = (2 \pm 1) \times 10^2$ μs.

Figure 6 shows a plot of the charge-carrier lifetime for a CH_3-terminated surface and the amount of surface oxide vs time as measured by XPS. In the first 200 h after alkylation, the lifetime
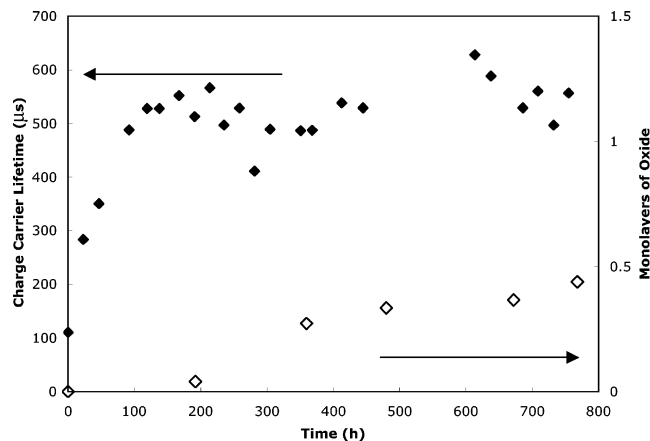
Figure 6. Plot of charge-carrier lifetime and monolayers of oxide vs time for CH_3-terminated Si(100) surfaces exposed to air.

rose from ∼100 to ∼500 μs, with little surface oxidation. Over the next 3 weeks the charge-carrier lifetime was constant even as the surface began to oxidize. After one month of exposure to air, the surface exhibited ∼0.5 monolayer of oxide, but no change was observed in τ.

D. Soft X-ray Photoelectron Spectroscopy. Figure 7 shows the soft X-ray photoelectron spectroscopy (SXPS) data recorded on the H-terminated Si(100) surface. The data in the figure depict the Si 2p region after the Si $2p_{1/2}$ component of the spin−orbit doublet had been removed from the data. Removal of the second peak of each doublet allowed for simpler and more accurate fitting of the peaks for each of the distinct Si species present. The spectrum showed a large peak with two shoulders at higher energy, and was well-fitted by four Voigt functions with peak energies of 0, 0.2, 0.5, and 0.9 eV (see Discussion).

Figure 8 shows the spin-orbit doublet-stripped SXPS Si 2p spectrum of the Cl-terminated Si(100) surface. The lowest energy emission was assigned to bulk silicon while peaks at 0.9, 1.9, and ∼3 eV higher in energy were observed. The spectrum was well-fitted by five Voigt functions with peak energies of 0.0, 0.4, 0.9, 1.9, and ∼3 eV (see Discussion).

Figure 9 show the spin−orbit doublet-stripped SXPS Si 2p spectrum of the CH_3-terminated Si(100) surface. The lower energy emission was assigned to bulk silicon, while a shoulder at 0.4 and peaks at 0.9 and 1.5 eV higher binding energy were observed. The spectrum was well-fitted by four Voigt functions (see Discussion).

IV. Discussion

A. Passivation of Si(100) Surfaces by Chlorination/Alkylation. The alkyl groups investigated herein ranged from the smallest saturated alkyl chain, methyl, to groups having increased steric bulk, such as ethyl and then phenyl. The alkyl groups used herein clearly did not bond to all possible atop sites on the Si(100) surface. The high-resolution XPS data for the C 1s region indicated that as the alkylating groups increased in size and steric bulk, the surface density of Si−C bonds decreased, leaving larger percentages of the surface unalkylated. Previous transmission IR studies[27,37] on Si(111) surfaces have indicated that Cl is completely removed from the surface by the Grignard exposure and subsequent reaction steps, leaving the detectable Si surface sites terminated either by Si−H or Si−C bonds. The XPS data described herein indicate that on the Si(100) surface, the two-step alkylation/chlorination also proceeds with complete removal of surficial Cl, even for sterically hindered alkyls. The lack of significant Si oxide on

Single-Crystal Silicon(100) Surfaces

J. Phys. Chem. B, Vol. 110, No. 30, 2006 **14775**
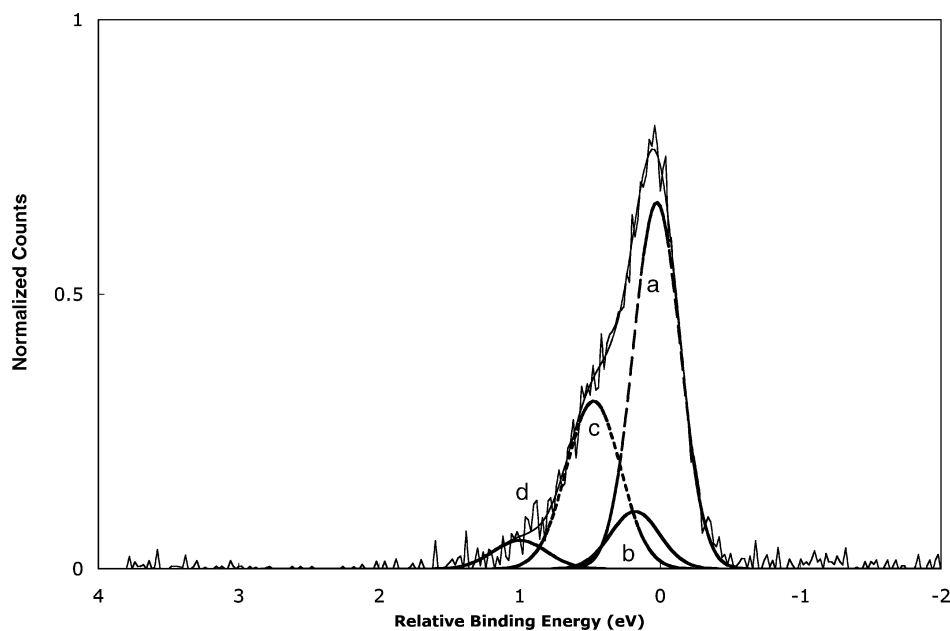
Figure 7. SXPS spectrum of the Si 2p region of H-terminated Si(100) surface after subtraction of spin−orbit doublets. The peak position is relative to bulk Si 2p. Four Voigt functions were fitted to the data. Fitted peaks were assigned to (a) bulk Si, (b) H−Si, (c) H$_2$Si, and (d) H$_3$Si surface species.
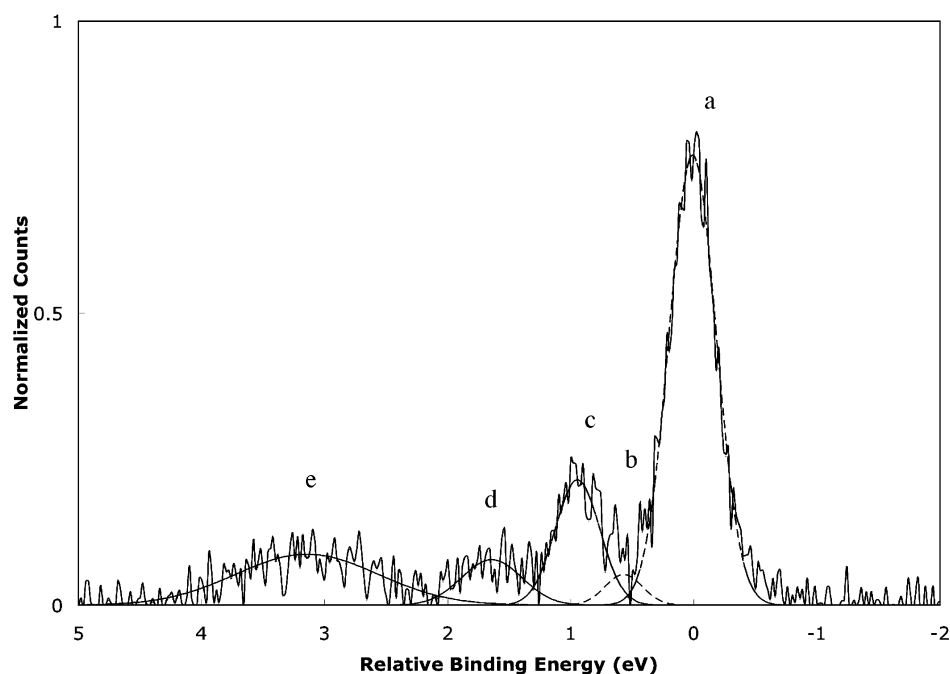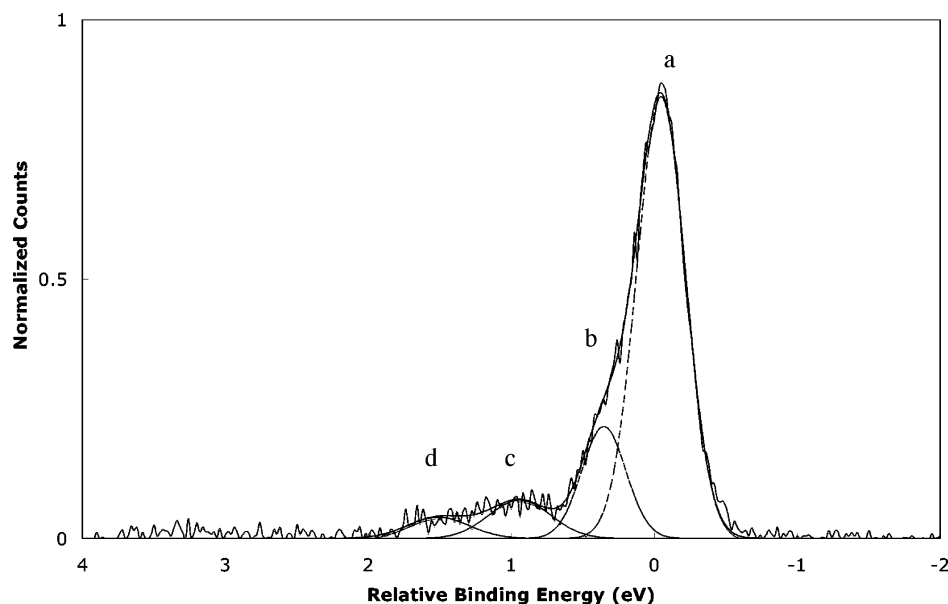

Figure 8. SXPS spectra of the Si 2p region for Cl-terminated Si(100) after subtraction of spin−orbit doublets. Peak positions are reported relative to the bulk Si 2p signal. Voigt functions were fitted to the data, and peaks were assigned to (a) bulk silicon, (b) SiH$_2$, (c) ClSi, (d) Cl$_2$Si, and (e) SiO$_x$ surface species.

such surfaces suggests that the surface is predominantly terminated by Si−C and Si−H bonds, as is the case for Si-(111) surfaces subjected to the same two-step reaction sequence.[27,32]

The presence of H-termination of unalkylated Si(100) surface sites would provide an explanation for the low S values observed for such systems. Si(111) surfaces carefully prepared with fluoride etches and terminated with H have been observed to have low densities of surface-localized electronic recombination centers, resulting in low surface recombination velocities.[38] CH$_3$-terminated Si(111) surfaces prepared through chlorination/alkylation have also shown low surface recombination velocities.[24,28] An alkylated Si(100) surface that contained both Si−H

and Si−C groups might therefore be expected to exhibit low surface recombination velocities, in accord with the observations.

The various alkylated Si(100) surfaces oxidized relatively slowly in air. The initial level of oxygen, detected as an O 1s signal in the XPS survey scan, was consistently assigned to adventitious adsorbed hydrocarbons having oxygen bonded to carbon. Assuming that all of the O 1s signal is ascribed to SiO$_2$, the survey scan XPS data yielded an upper bound of 0.2 ML of SiO$_2$. The assignment of the O 1s signal to weakly adsorbed carbonaceous contamination is supported by the disappearance of signals arising from oxidized carbon, and a more well-defined Si 2p peak shape ascribable to Si bonded to carbon, in SXPS

Figure 9. SXPS spectrum of the Si 2p region of the CH$_3$-terminated Si(100) surface after subtraction of spin−orbit doublets. Peak positions are reported relative to the bulk Si 2p signal. Voigt functions were fitted to the data. The multiplicity of species present prevented assigning each peak to a unique surface species, and peaks were assigned to (a) bulk silicon, (b) CH$_3$−Si, CH$_3$−SiH, SiH, and SiH$_2$, (c) (CH$_3$)$_2$Si and SiH$_3$, and (d) (CH$_3$)$_3$Si surface species and/or silicon oxide.

studies of methyl-terminated Si(111) surfaces, after annealing of such surfaces at mild (600 K) temperatures.[36] A more stringent upper bound on the level of Si oxidation than the <0.2 ML of SiO$_2$ obtained from the XPS survey scan can be established by inspection of the Si 2p data in the high-resolution XPS and SXPS scans (Figures 3 and 9). The lower line in the inset of Figure 1 shows the Si 2p region for the silicon surface of Figure 1, while the upper line displays the Si 2p region of another Si(100) surface that was covered by 0.2 monolayer of oxide, as calculated from the ratio of the oxidized Si 2p peak area to the area of the bulk Si 2p signal in the high-resolution Si 2p XPS data. The significant difference between these two scans indicated that considerably less than 0.2 ML of oxide was present on the CH$_3$-terminated surface, supporting the conclusion that the O 1s peak observed in the survey scan was due primarily to adventitious oxygen (likely oxidized hydrocarbons) from the functionalization process and not from extensive oxidation of the Si surface. An even more stringent upper bound on the level of oxidized Si can be established by the lack of an oxidized Si 2p signal in the more surface-sensitive SXPS data, in which even 0.1 ML of SiO$_2$ or other Si oxides would have been readily detected (Figure 9). Further evidence that the oxygen 1s signal arose primarily from adventitous oxidized adsorbed hydrocarbons is that the ratio of the O 1s signal to the area of the 286.9 eV C 1s peak was in general accord with ratio of the O 1s and C 1s sensitivity factors, indicating that most of the detected oxygen is associated with oxygen bonded to carbon, as opposed to oxygen bonded to silicon.

For the alkyl groups investigated herein, at least partial inhibition of the rate of surface oxidation might be expected due to steric crowding of surficial Si−H bonds by neighboring alkyl groups. A modest degree of oxidative protection has been observed on Cu by forming self-assembled monolayers with use of very long chain alkylthiols to bond to the Cu surface,[39] indicating that steric bulk may contribute to the observed oxidative passivation of the alkylated Si surfaces. This crowding may inhibit the oxidation of Si−H sites because oxygen or water would need to intercalate into the alkyl surface overlayer to react with the surface. However, the very large difference

between the air oxidation rates of alkylated and H-terminated Si(100) surfaces (Figures 3 and 4) suggests that the reaction mechanism may involve multiple neighboring Si−H sites and/or oxidation spreading outward on the surface from imperfect passivation from either H- or C-termination caused by surface defects. Modest alkyl coverages on the surface may then be sufficient to reduce the observed rate of oxidation, by reduction of highly active, imperfectly passivated, surface sites. The data, however, clearly show that even partial coverage of alkyls is sufficient to endow a large degree of both electrical and chemical passivation to functionalized Si(100) surfaces.

B. Soft X-ray Photoelectron Spectra. Infrared absorption studies have demonstrated that the wet-chemically prepared, H-terminated Si(100) surface contains all three silicon-hydride species (Figure 5).[22,26] Accordingly, the largest Si 2p SXPS peak, at the lowest binding energy, was assigned to bulk Si, whereas the peak 0.2 eV higher in energy than the bulk Si peak was attributed to the Si−H species. This peak position is consistent with the 0.15 eV shift of Si−H relative to bulk Si observed on the well-defined, monohydride-terminated Si(111) surface.[32,40,41] The peaks at 0.5 and 0.9 eV higher than the bulk peak were assigned to SiH$_2$ and SiH$_3$, respectively. The increasingly positive peak shifts for the dihydride and trihydride species are consistent with expectations for the Si becoming more electropositive as additional hydrogens are bonded to the Si. The data for the H-terminated Si(100) surface indicated that a large fraction (68%) of the surface was SiH$_2$, with 21% SiH and 11% SiH$_3$, for the two samples measured (Table 3).

H-terminated Si(100) surfaces measured by SXPS showed relative coverages of SiH, SiH$_2$, and SiH$_3$ that were consistent with the IR absorbance spectra, as well as with thermal desorption measurements.[23,26,42] However, the peak fitting relied on constraining the fitting such that the relative peak separation was predefined by using SXPS measurements of the H−Si-(111) surface, as well as limiting the full width at half maximum for the SiH and SiH$_2$ signals to be within 20% of each other.[32]

Figure 8 shows the doublet-stripped SXPS Si 2p spectrum of the Cl-terminated Si(100) surface. The lowest energy emission

Single-Crystal Silicon(100) Surfaces

J. Phys. Chem. B, Vol. 110, No. 30, 2006 **14777**

TABLE 3: Relative Integrated Area for Peak Fits of SXPS Data of Functionalized Si(100) Surfaces[a]

X	ML SiX	ML SiX$_2$	ML SiX$_3$/(SiO$_x$)	ML SiH$_2$
−H	0.21	0.68	0.11	
−Cl	0.34 ± 0.08	0.18 ± 0.08	0.41 ± 0.06	0.03 ± 0.02
−CH$_3$	0.82 ± 0.08	0.10 ± 0.05	0.08 ± 0.05	
−C$_2$H$_5$	0.79	0.11	0.09	
−CH$_2$C$_6$H$_5$	0.81	0.11	0.08	

[a] SiH, SiC$_2$H$_5$, and Si−CH$_2$C$_6$H$_5$ represent two averaged values for each column. SiCl entries are for six measurements, and SiCH$_3$ entries are for eight measurements. SiX represents the fraction of ML resulting from singly bonded −X. For SiCl, a SiH$_2$ peak was fitted to the spectra in addition to the SiCl peak.

peak was assigned to bulk silicon, while the peak 0.9 eV higher in energy was assigned to monochlorinated species, such as SiCl. This peak position is in excellent agreement with the shift that has been observed for well-defined, monochloride-terminated, Cl−Si(111) surfaces.[30,32] A smaller peak, 0.4 eV higher in energy than bulk silicon, was added to account for any SiH$_2$. While addition of this peak produced only a small improvement in the overall fit of the data, it noticeably improved the fit of the low-binding energy edge of the SiCl peak. The peaks 1.9 and ∼3 eV higher than the energy of the bulk Si were assigned to dichlorinated species such as SiCl$_2$, and to Si oxides, respectively. The oxide likely arose because these samples were prepared and transported to the spectrometer in air. Analysis of the relative peak areas indicated that 34 ± 8% of the surface was monochlorinated and 18 ± 8% was dichlorinated (Table 3). The formation of SiCl$_3$ was not expected, because of the large size of Cl atoms. A peak due to SiCl$_3$ would be partially obscured by the oxide peak, which accounted for 41 ± 6% of the surface silicon atoms. The quality of the fit could not be significantly improved by adding a peak representing SiCl$_3$ at ∼2.5 eV above bulk Si nor did the SiO$_x$ peak appear to contain a significant low-energy component. Hence, a relatively small amount of SiCl$_3$ was apparently present on the surface.

No additional signals, such as those potentially arising from HSiCl, H$_2$SiCl, HSiCl$_2$, or SiH$_3$, were used to fit the peaks, as these species are expected to have peak positions very close to those already used. The SiH$_2$ peak comprised less than 5% monolayer equivalent coverage. However, its inclusion points to residual Si−H bonds on the surface, indicating that the monochlorinated Si peak may contain contributions from other species such as HSiCl and H$_2$SiCl, while the dichlorinated Si peak may contain contributions from SiCl$_2$, HSiCl$_2$, and H$_2$SiCl$_2$.

The alkylated Si(100) surfaces showed similar SXPS features to those observed for the H-terminated Si(100) surface. Figure 9 shows the spin−orbit doublet stripped spectrum of a CH$_3$-terminated Si(100) surface. The peak 0.4 eV higher than the bulk Si emission was assigned to Si−CH$_3$, as well as to other surface species with similar peak positions, such as SiH and SiH$_2$. The 0.4 eV shift from the bulk silicon emission is similar to the 0.4 eV shift observed for SiH$_2$ on H−Si(100) surfaces (Figure 7), and is similar to the 0.3−0.4 eV shift that has been observed for Si−C species in previous studies of the well-defined, methyl-terminated, CH$_3$−Si(111) surface performed on the same instrumentation used here.[32] The emission at 0.9 eV was attributed primarily to signals arising from H$_2$SiCH$_3$, Si-(CH$_3$)$_2$, and HSi(CH$_3$)$_2$, with a possible contribution by Si(I) oxide, whereas the peak at 1.5 eV is assigned to Si(CH$_3$)$_3$ and/or a contribution from Si(II) oxide.

The SXPS data for C$_2$H$_5$-terminated Si(100) surfaces were similar to the data for the CH$_3$-terminated Si(100) surface,

exhibiting a prominent emission shifted 0.3 eV from the bulk Si peak. This peak was assigned to singly C$_2$H$_5$-terminated Si, SiH, and SiH$_2$ surface species. The smaller energy shift of the peak relative to that observed for Si−CH$_3$ on CH$_3$−Si(100) is consistent with the C$_{Si}$ 1s signals which also indicate that SiH and/or SiH$_2$ comprise larger fractions of the C$_2$H$_5$−Si(100) surface than of the CH$_3$−Si(100) surface. C$_6$H$_3$CH$_6$-terminated Si(100) samples also showed similar SXPS spectra to C$_2$H$_5$−Si(100) surfaces, with the first surface emission shifted by 0.3 eV from the Si bulk, again suggesting the presence of significant amounts of SiH and/or SiH$_2$ on such surfaces, as well as Si−alkyl bonds as evidenced by the C$_{Si}$ 1s emission and the chemically shifted Si 2p emission.

For the alkylated surfaces, the SXPS peak fitting resulted in an emission shifted 0.3−0.4 eV higher than the bulk Si that could contain contributions from several surface species. The first peak higher in energy than the bulk peak for an alkylated sample could arise from SiH, SiR, SiH$_2$, and HSiR, while SiR$_2$, HSiR$_2$, H$_2$SiR, SiH$_3$, and SiR$_3$ are expected to contribute to the intensity of the two peaks at higher binding energy. Since the XPS survey scans showed no evidence for the Cl 2s or 2p peaks after alkylation, these higher energy peaks do not involve contributions from chlorinated Si species.

V. Conclusions

After chlorination of H-terminated Si(100) surfaces, all of the surface-bound Cl was removed by functionalization of the Si surface with alkyl Grignard reagents, even when very bulky alkyl Grignard reagents were used. Alkylation of Si(100) surfaces through this two-step chlorination/alkylation procedure produced both chemical and electrical passivation of the Si surface, even though only a fraction of the surface sites were functionalized by Si−C alkyl bonds. The intensity of a low binding energy C 1s XPS peak, ascribable to carbon bonded to Si, provided a quantitative estimate of the coverage of alkyls on such surfaces relative to the coverage of methyl groups on CH$_3$-terminated Si(100) surfaces. Functionalization with −C$_2$H$_5$ groups yielded 60% of the coverage of carbon-bonded Si relative to carbon-bonded Si on CH$_3$-terminated Si(100) surfaces, whereas bulkier and longer alkyl groups resulted in even lower coverages of carbon-bonded Si species. Even −C$_6$H$_5$ groups, which were measured by XPS to produce only 40% of the coverage of carbon-bonded Si sites as were found on the CH$_3$-terminated Si(100) surface, showed excellent surface passivation, with less than half a monolayer of Si oxide formed on the surface after three weeks exposure to air, and with surface recombination velocities <60 cm s^{-1} after that same time period. Soft X-ray photoelectron spectra of the Si(100) surface indicated that while the predominant spectroscopically detectable species on the wet-chemically etched Si(100) surface was SiH$_2$, the chlorinated Si(100) surface was primarily terminated by monochloro (i.e., SiCl and HSiCl) species. All alkylated surfaces displayed mutually similar SXP spectra, indicating that these surfaces were primarily terminated with Si−alkyl, SiH, and SiH$_2$ species. These surfaces demonstrated robust charge-carrier lifetimes for periods approaching one year of exposure to air.

Nemanick et al.

10866, and the Beckman Institute Molecular Materials Research Center at the California Institute of Technology.

References and Notes

(1) Buriak, J. M. *Chem. Rev.* **2002**, *102*, 1271.

(2) Buriak, J. *Chem. Commun.* **1999**, 1051−1060.

(3) Haber, J. A.; Lauermann, I.; Michalak, D.; Vaid, T. P.; Lewis, N. S. *J. Phys. Chem. B* **2000**, *104*, 9947−9950.

(4) Stewart, M. P.; Robins, E. G.; Geders, T. W.; Allen, M. J.; Choi, H. C.; Buriak, J. M. *Phys. Status Solidi A* **2000**, *182*, 109−115.

(5) Linford, M. R.; Chidsey, C. E. D. *J. Am. Chem. Soc.* **1993**, *115*, 12631−12632.

(6) Linford, M. R.; Fenter, P.; Eisenberger, P. M.; Chidsey, C. E. D. *J. Am. Chem. Soc.* **1995**, *117*, 3145−3155.

(7) Terry, J.; Linford, M. R.; Wigren, C.; Cao, R. Y.; Pianetta, P.; Chidsey, C. E. D. *Appl. Phys. Lett.* **1997**, *71*, 1056−1058.

(8) Terry, J.; Mo, R.; Wigren, C.; Cao, R. Y.; Mount, G.; Pianetta, P.; Linford, M. R.; Chidsey, C. E. D. *Nucl. Instrum. Methods Phys. Res.*, *Sect. B* **1997**, *133*, 94−101.

(9) Effenberger, F.; Gotz, G.; Bidlingmaier, B.; Wezstein, M. *Angew. Chem.*, *Int. Ed.* **1998**, *37*, 2462−2464.

(10) Stewart, M. P.; Buriak, J. M. *Angew. Chem.*, *Int. Ed.* **1998**, *23*, 3257.

(11) Sieval, A. B.; Demirel, A. L.; Nissink, J. W. M.; Linford, M. R.; van der Maas, J. H.; de Jeu, W. H.; Zuilhof, H.; Sudholter, E. J. R. *Langmuir* **1998**, *14*, 1759−1768.

(12) Sung, M. M.; Kluth, G. J.; Yauw, O. W.; Maboudian, R. *Langmuir* **1997**, *13*, 6164−6168.

(13) Zazzera, L. A.; Evans, J. F.; Deruelle, M.; Tirrell, M.; Kessel, C. R.; Mckeown, P. *J. Electrochem. Soc.* **1997**, *144*, 2184−2189.

(14) Buriak, J. M.; Allen, M. J. *J. Am. Chem. Soc.* **1998**, *120*, 1339−1340.

(15) Buriak, J. M.; Allen, M. J. *J. Lumin.* **1998**, *80*, 29−35.

(16) Holland, J. M.; Stewart, M. P.; Allen, M. J.; Buriak, J. M. *J. Solid State Chem.* **1999**, *147*, 251−258.

(17) Henry de Villeneuve, C.; Pinson, J.; Ozanam, F.; Chazalviel, J. N.; Allongue, P. In *Mater. Res. Soc. Symp. Proc.* **1997**, *451*, 185−195.

(18) Vieillard, C.; Warntjes, M.; Ozanam, F.; Chazalviel, J.-N. *Proc. Electrochem. Soc.* **1996**, *95*, 250.

(19) Bansal, A.; Li, X.; Lauermann, I.; Lewis, N. S.; Yi, S. I.; Weinberg, W. H. *J. Am. Chem. Soc.* **1996**, *118*, 7225−7226.

(20) Juang, A.; Scherman, O. A.; Grubbs, R. H.; Lewis, N. S. *Langmuir* **2001**, *17*, 1321−1323.

(21) Royea, W. J.; Juang, A.; Lewis, N. S. *Appl. Phys. Lett.* **2000**, *77*, 1988−1990.

(22) Chabal, Y. J.; Higashi, G. S.; Ragahavchari, K.; Burrows, V. A. *J. Vac. Sci. Technol. A* **1989**, *A7*, 2104.

(23) Niwano, M.; Takeda, Y.; Ishibashi, K.; Kurita, K.; Miyamoto, N. *J. Appl. Phys.* **1992**, *71*, 5646.

(24) Webb, L. J.; Lewis, N. S. *J. Phys. Chem. B* **2003**, *107*, 5404−5412.

(25) Bansal, A.; Lewis, N. S. *J. Phys. Chem. B* **1998**, *102*, 1067−1070.

(26) Chyan, O. M. R.; Wu, J.; Chen, J.-J. *Appl. Spectrosc.* **1997**, *51*, 1905.

(27) Nemanick, E. J.; Hurley, P. T.; Brunschwig, B. S.; Lewis, N. S. *J. Phys. Chem. B*, in press.

(28) Bansal, A.; Li, X. L.; Yi, S. I.; Weinberg, W. H.; Lewis, N. S. *J. Phys. Chem. B* **2001**, *105*, 10266−10277.

(29) Seah, M. P. In *Practical Surface Analysis*, 2nd ed.; Briggs, D., Seah, M. P., Eds.; John Wiley & Sons: Chichester, UK, 1990; Vol. 1, pp 201−255.

(30) Terry, J.; Linford, M. R.; Wigren, C.; Cao, R. Y.; Pianetta, P.; Chidsey, C. E. D. *J. Appl. Phys.* **1999**, *85*, 213−221.

(31) Liu, H. B.; Hamers, R. J. *Surf. Sci.* **1998**, *416*, 354−362.

(32) Webb, L. J.; Nemanick, E. J.; Biteen, J. S.; Knapp, D. W.; Michalak, D. J.; Traub, M. C.; Chan, A. S. Y.; Brunschwig, B. S.; Lewis, N. S. *J. Phys. Chem. B* **2005**, *109*, 3930−3937.

(33) Sze, S. M. *The Physics of Semiconductor Devices*, 2nd ed.; Wiley: New York, 1981.

(34) Dabrowski, J.; Mussig, H. J. *Silicon Surfaces and Formation of Interfaces*; World Scientific Publishing Co. Pte. Ltd.: London, UK, 2000.

(35) Durbin, T. D.; Simpson, W. C.; Chakarian, V.; Shuh, D. K.; Varekamp, P. R.; Lo, C. W.; Yarmoff, J. A. *Surf. Sci.* **1994**, *316*, 257−266.

(36) Hunger, R.; Fritsche, R.; Jaeckel, B.; Jaegermann, W.; Webb, L. J.; Lewis, N. S. *Phys. Rev. B* **2005**, *72*.

(37) Rivillon, S.; Chabal, Y.; Webb, L. J.; Michalak, D. J.; Lewis, N. S.; Halls, M. D.; Ragahavchari, K. *J. Vac. Sci. Technol. A* **2005**, *23*, 1100−1106.

(38) Yablonovitch, E.; Allara, D. L.; Chang, C. C.; Gmitter, T.; Bright, T. B. *Phys. Rev. Lett.* **1986**, *57*, 249−252.

(39) Laibinis, P. E.; Whitesides, G. M. *J. Am. Chem. Soc.* **1992**, *114*, 1990−1995.

(40) Bjorkman, C. H.; Alay, J. L.; Nishimura, H.; Fukuda, M.; Yamazaki, T.; Hirose, M. *Appl Phys. Lett.* **1995**, *67*, 2049−2051.

(41) Karlsson, C. J.; Owman, F.; Landemark, E.; Chao, Y. C.; Marstensson, P.; Uhrberg, R. I. G. *Phys. Rev. Lett.* **1994**, *72*, 4145−4148.

(42) Thanh, V. L.; Bouchier, D.; Hincelin, G. *J. Appl. Phys.* **2000**, *87*, 3700.